Supporting Information

^{19}F electron nuclear double resonance (ENDOR) spectroscopy for distance measurements using a trityl spin labels in DNA duplexes

N.B. Asanbaeva[a], D.S. Novopashina[b], O.Yu. Rogozhnikova[a], V.M. Tormyshev[a], A. Kehl[d], A.A. Sukhanov[c], A.V. Shernyukov[a], A.M. Genaev[a], A.A. Lomzov[b], M. Bennati[d,e], A. Meyer[d,e], E.G. Bagryanskaya[a*]

[a]*N. N. Vorozhtsov Novosibirsk Institute of Organic Chemistry SB RAS, 9 Pr. Ak. Lavrentjeva, Novosibirsk 630090, Russia*

[b]*Institute of Chemical Biology and Fundamental Medicine SB RAS, 8 Pr. Ak. Lavrentjeva, Novosibirsk 630090, Russia*

[c]*Zavoisky Physical-Technical Institute, FRC Kazan Scientific Center of RAS, 10/7 Sibirsky Tract, Kazan 420029, Russia*

[d]*Research Group EPR Spectroscopy, Max Planck Institute for Multidisciplinary Science, Am Fassberg 11, 37077 Göttingen, Germany*

[e]*Institute of Physical Chemistry, Department of Chemistry, Georg August University of Göttingen, Tammannstr.6, Göttingen, Germany*

Content

X-BAND CW EPR SPECTRA **3**

ECHO DETECTED EPR SPECTRA **3**

TEST OF NUCLEAR FREQUENCY OVERLAP IN Q-BAND MIMS ENDOR SPECTRA **4**

RELAXATION TIMES MEASUREMENTS **4**

MIMS ENDOR SPECTRA SIMULATION PROCEDURE **4**

BLIND SPOTS AND T VALUE ADJUSTMENT **6**

MOLECULAR DYNAMICS SIMULATION **7**

PREPARATION OF NON-STANDARD PARAMETERS 7

MD-SIMULATIONS IN EXPLICIT WATER SHELL 9

FIGURE S6: "UNMODIFIED" DNA-DUPLEX DNA20-1 10

FIGURE S7: FLUORINE LABELED DNA-DUPLEX DNA20-F1 11

FIGURE S8. F- AND FINLAND TRITYL LABELED DNA-DUPLEX FIN-DNA-20-F1 (T=1600NS) 12

FIGURE S9. F- AND FINLAND TRITYL LABELED DNA-DUPLEX FIN-DNA-20-F1 (T=2500NS) 13

FIGURE S10. F- AND OX063 LABELED DNA-DUPLEX OXO-DNA-20-F1 (T=2500NS) 14

FIGURE S11. "UNMODIFIED" DNA-DUPLEX DNA20-2 15

FIGURE S12. FLUORINE LABELED DNA-DUPLEX DNA20-F2 15

FIGURE S13. F- AND FINLAND TRITYL LABELED DNA-DUPLEX FIN-DNA-20-F2 (T=2000NS) 16

FIGURE S14. F- AND OXO63 LABELED DNA-DUPLEX OX0-DNA-20-F2 (T=2500NS) 17

REFERENCES **19**

X-band CW EPR spectra

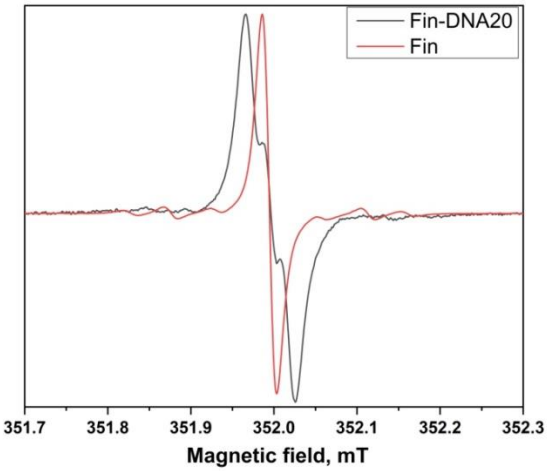

Figure S1. Comparison of the EPR spectra of the free label Fin (red line) and the trityl-labeled Fin-DNA20 oligonucleotide (black line).

The X-band (9 GHz) CW EPR spectrum of free Fin radical in water solution at 300 K consists of a single narrow EPR line (Figure S1). The covalent attachment of Fin label to functionalized oligonucleotide leads to the following changes in CW EPR spectra (Figure S1): to a line broadening due to increase of tumbling correlation time and to the appearance of a triplet splitting of EPR line induced by hyperfine interaction with the piperazine nitrogen.

Echo detected EPR spectra

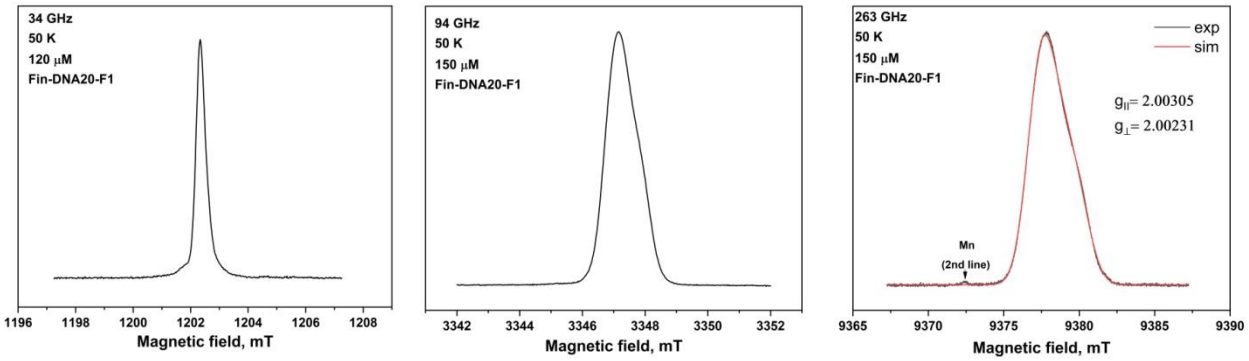

Figure S2. Echo detected EPR spectra of Fin-DNA-20-F1 at different frequencies

Echo detected EPR spectra of Fin-DNA-20-F1 were recorded at 34, 94 and 263 GHz (Figure S2). In contrast to nitroxides, the spectra of trityl do not show strong *g* anisotropy. As the strength of the magnetic field increases, the main line mainly broadens. Subsequently, all pulsed ENDOR experiments were carried out at the position of the magnetic field in resonance with the maximum echo signal. Only for a frequency of 263 GHz, experiments were carried out at several positions in the field. It was shown that the obtained ENDOR spectra are almost identical.

Test of nuclear frequency overlap in Q-band Mims ENDOR spectra

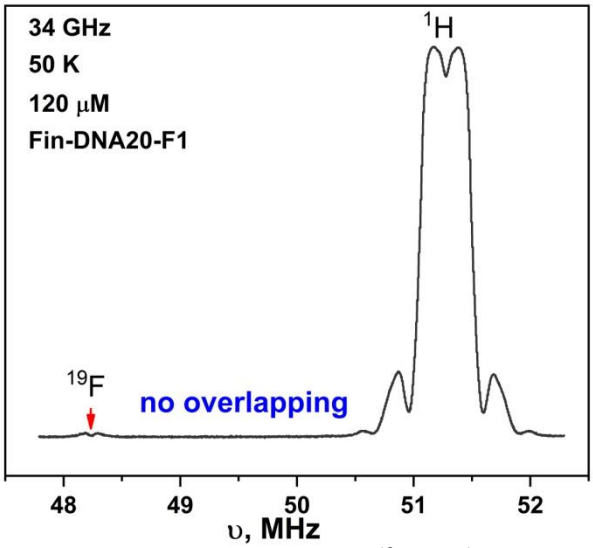

Figure S3. Mims ENDOR frequency sweep across the region of ^{19}F and ^{1}H nuclear frequencies at 34 GHz for Fin-DNA20-F1. The ^{19}F resonances are not overlapping with the ^{1}H resonances.

Relaxation times measurements

The spin-lattice relaxation time of the electron T_{1e} determines the shot repetition rate and was measured using inversion recovery experiments (π-t-π/2-τ-π-τ).

T_M is often measured using the two-pulse (π/2-τ-π-τ) echo experiment. However, T_M in Mims ENDOR depends strongly also on the time interval T (between second and third MW pulses) Therefore, T_M was measured by monitoring the intensity of the stimulated echo when varying τ for different, fixed values of T. The procedure was described in Ref. [1].

Table S1. The fitting parameters of the echo decay curves at 50 K (34 GHz). Values were extracted from the echo decay curve by using a mono exponential fitting function.

Sample	T_{1e}, ms	T, μs	T_M, μs
Fin-DNA20-F1	7.3	61	1.49
Fin-DNA20-F2	6.7	61	1.09
OX063-DNA20-F1	9.1	61.5	1.51
OX063-DNA20-F2	8.4	61	2.28

Mims ENDOR spectra simulation procedure

Mims ENDOR (34 GHz) simulations were carried out with the *EasySpin* software. The spectra were simulated using the approximation of a Gaussian distribution of distances with a center R_0 and a width σ that were recalculated to *hf* couplings. For each R value in the range [R_0-

3σ; R_0+3σ], the Mims ENDOR spectrum was modeled and then all spectra were summed with the appropriate weights:

$$w = \frac{1}{\sqrt{2\pi\sigma^2}} * e^{-\frac{(R-R_0)^2}{2\sigma^2}} \quad \textbf{Eq.1}$$

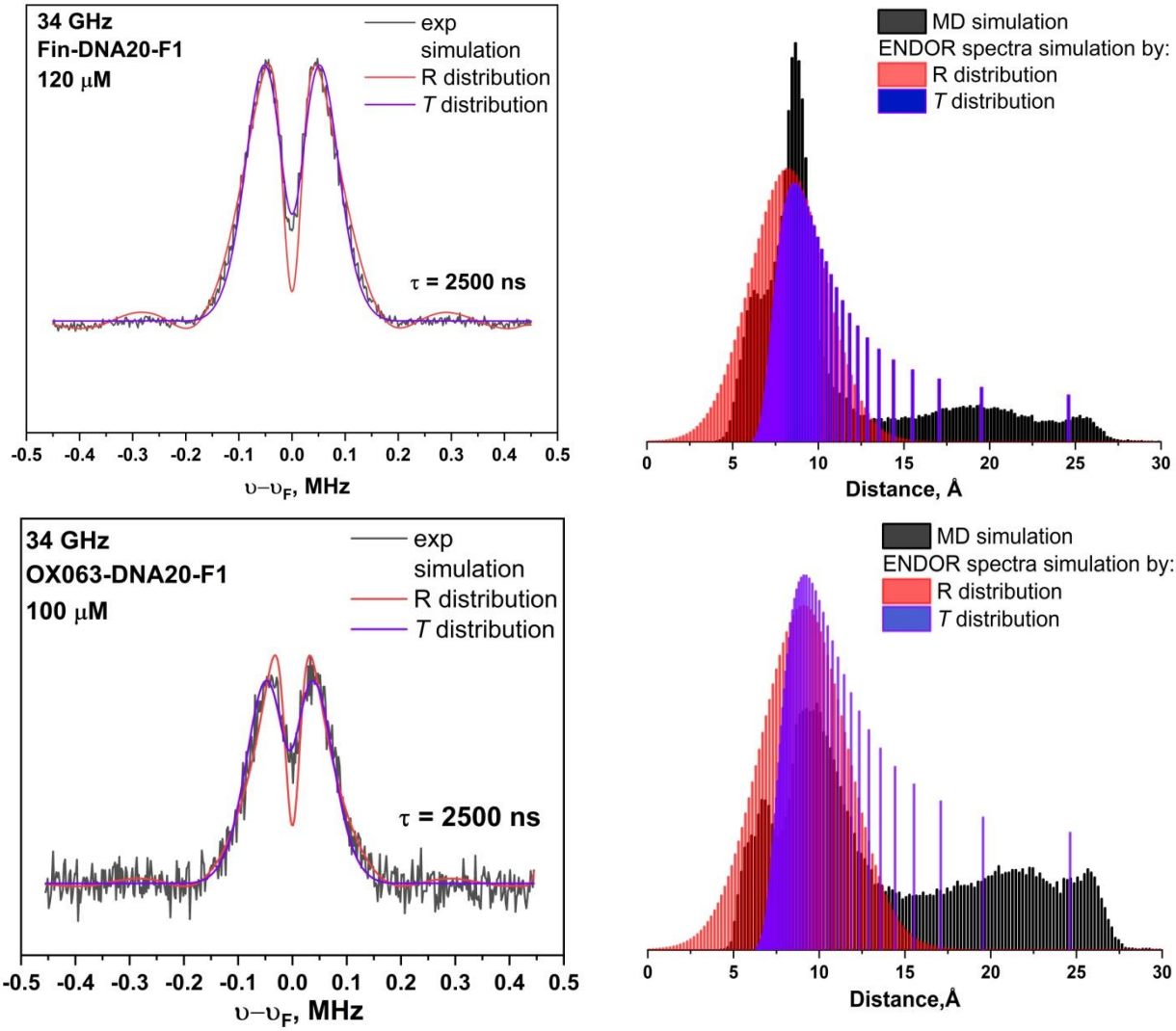

Figure S4. Experimental and simulated 34 GHz Mims ENDOR spectra of Fin-DNA20-F1 (**top**) and OX063-DNA20-F1 (**bottom**); the corresponding distance distributions are shown on the right

Table S2. Results of simulation 34 GHz Mims ENDOR spectra

Sample	τ, ns	T_{read}, MHz	R_{read}, Å	R_{sim}, Å ± σ	T_{sim}, MHz ± σ
Fin-DNA20-F1	2500	0.09 ± 0.01	9.3 ± 0.4	8.2 ± 2.2	0.12 ± 0.06
	1600	0.11 ± 0.01	8.9 ± 0.3	8.2 ± 2.0	0.14 ± 0.07
Fin-DNA20-F2	2000	0.04 ± 0.01	12.1 ± 1.1	12.9 ± 2.9 (60%) 8.6 ± 2.2 (40%)	0.04 ± 0.02 (60%) 0.12 ± 0.08 (40%)

OX063-DNA20-F1	2500	0.08 ± 0.01	9.7 ± 0.5	9.1 ± 2.5	0.10 ± 0.06
	1000	0.09 ± 0.01	9.4 ± 0.4	-	
OX063-DNA20-F2	2500	0.03 ± 0.01	14.4 ± 3.4	-	

As can be seen from the modeling results (Figure S4, Table S2), we can choose the distribution satisfactorily describing experimental data. The distance of the $\boldsymbol{R}_{\text{read}}$ enters the range, but the distribution center can be shifted by almost 1 Å. The problem is most likely that we use only one Gaussian distribution for description. If we use simulation with Gaussian distribution of *T* values (weights were calculated similarly to Eq. 1) we get a better fit with the experimental spectra (Figure S4). The resulting Gaussian distribution *T* values corresponds to a complex (non Gaussian) distance distribution curve (violet diagram on Figure S4, right). As shown by the results of MD simulation (black diagram) the range of possible distances is a more complex distribution.

Blind spots and τ value adjustment

Mims ENDOR experiment produces blind spots in the spectrum according to the function[2]:

$$F = 0.5 \times \sin^2(\pi \cdot \nu_{HFC} \cdot \tau)$$

where *F* is the ENDOR efficiency, τ is time between the two 90° preparation pulses, and ν_{HFC} represents the expected coupling frequency. Thus, we can calculate the positions of blind spots as ± 500/τ MHz (τ in ns) and the τ values have to be optimized for each sample to detect the peaks of the dipolar powder pattern (Pake pattern), with principal axes frequencies at $\nu_{HFC} = \pm T$.

Molecular dynamics simulation

Preparation of non-standard parameters

For geometry optimizations and energy calculations was used r^2SCAN-3c[3] method implemented in ORCA 5.0.3[4] software. This method has a high accuracy to resources and calculation time ratio[5] and perfectly reproduces the experimental geometric parameters of trityl radicals taken from the X-ray diffraction data (the Cambridge Structural Database entries: ESECUB and TIXCEJ). The QM electrostatic potential was evaluated at the ROHF/6-31G* level of theory by using GAMESS[6] software. Charge derivation was made by two stages constrained RESP-fitting of a set of 3-5 low-energy conformers using Antechamber included in the AmberTools21[7] package.

The parameters fitting was carried out using the mdgx utility included in the package AmberTools21[7]. The parametrization of the trityl fragment was carried out on the basis of the GAFF force field (Version 1.81). For this purpose, a new type of carbon atom "ct" describing the central carbon atom in the triaryl methane (TAM) type radicals was introduced. The simplest TAM radical (the Gomberg radical) was used for parametrization due to its symmetry and small size. The result of two-stage fitting is shown in the Figure S5. At the first iteration, the equilibrium values of bond length and bond angle, as well as bond, angle, and dihedral stiffness, were fitted based on a set of QM structures (in which the corresponding geometric parameters were varied using a relaxed scanning procedure). An excellent correlation between the energies of the MM and QM and very close structures of the minimum were obtained. But the process of racemization (M-/P- propeller transition by means of two-flip process) proceeded faster than it follows from the QM calculation (MD barrier ~5 kcal/mol, QM 8.5 kcal/mol). The alternative higher energy transition state (TS) corresponding to the one-flip process (not included in the fit) differed greatly in energy due to very close protons of neighboring aromatic rings (~1.6 Å, large contribution from the Lenard-Jones potential). Only the dihedral stiffness was fitted at a second iteration, which had additional structures of MM dihedral scan and MD two-flip TS. As a result, with the obtained parameters, the rate of the racemization process became close to the QM prediction and corresponded to the barrier of ~9 kcal/mol.

It was found that the properties of the piperazine linker are poorly described by the GAFF field. Thus, the twist conformer had a lower energy than the chair conformer (~ 1 kcal/mol, cf 2.5 kcal/mol in favor of chair by QM) and the amide bond *cis*-/*trans*- isomerization was easier than expected. Therefore, the corresponding dihedral stiffness parameters have also been reparameterized by mdgx. After that, the chair conformer became even more stable compared to the QM (by 2.0 kcal/mol), but given the low population of the twist conformer and the fact that

the chair-chair and *cis-/trans-* transition processes had the expected rates, a more extended parameterization was not carried out further and obtained parameters were used as is.

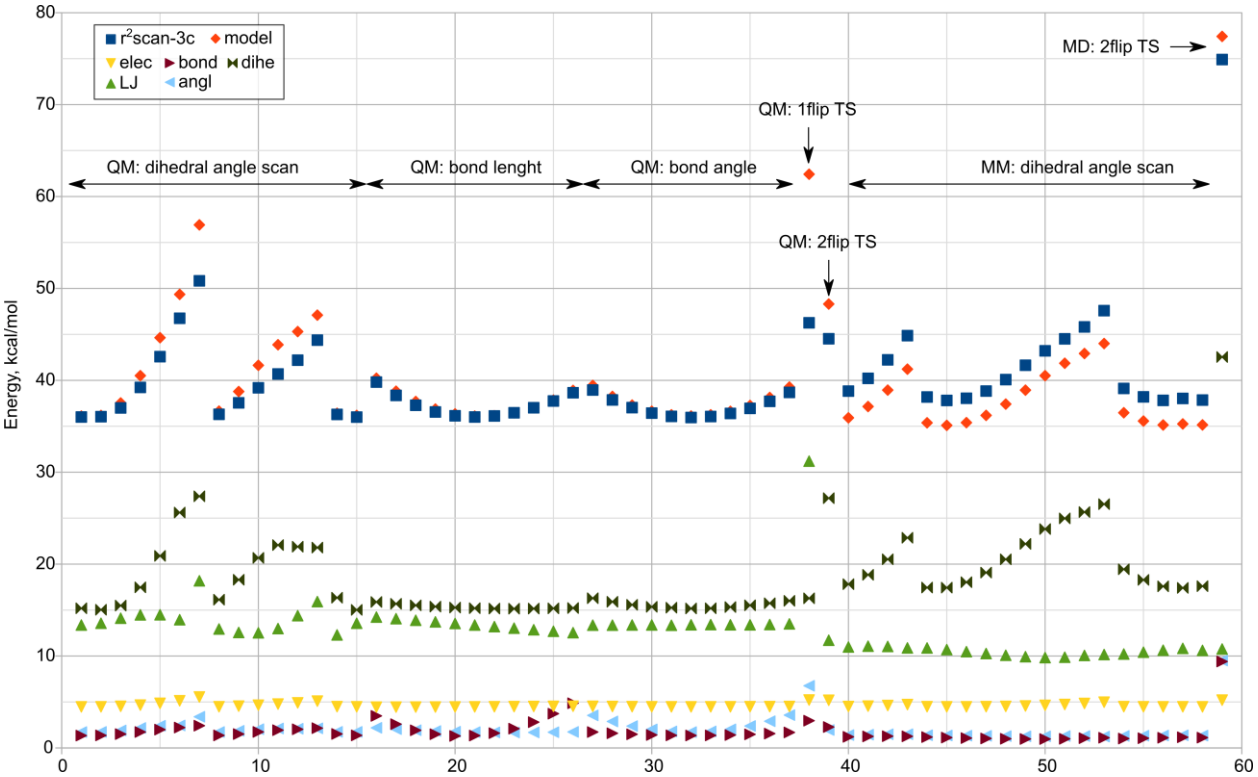

Figure S5. Results of two-stage fitting of the Gomberg radical parameters by the mdgx utility. The figure shows corrected to average energy values QM (blue rectangles), MM (red diamonds) and corresponding MM energy contributions (elec – electrostatic term; bond – bond term; dihedral – dihedral term; LJ - Lennard-Jones term ; angle - angle term).

The content of the frcmod-file used for MD-calculations is given below:

```
MASS
ct 12.010         0.360

BOND
ca-ct   252.12    1.431
os-CI   320.00    1.410

ANGLE
ca-ct-ca    40.311      114.56
ca-ca-ct    64.000      121.11
c -os-CI     60.0       117.00
os-CI-H1     50.0       109.50
os-CI-CT     50.0       109.50
F -CT-CE     50.0       109.00

DIHEDRAL
X -ca-ct-X     1     2.035        180.0              2.0
ca-ca-ca-ct    4    14.500        180.0              2.0
X -ca-c -X     1     1.582        180.0              2.0
```

```
n -c3-c3-n    1    0.505       0.0              3.0
c3-c3-n -c3   1    1.278       0.0              3.0
c3-n -c -o    1    2.565       180.0            2.0
c3-n -c -ca   1    2.515       180.0            2.0
c3-n -c -os   1    2.550       180.0            2.0
X -CI-os-X    3    1.150       0.0              3.0
H1-CE-CT-F    1    0.000       0.0             -3.0
H1-CE-CT-F    1    0.190       0.0              1.0

IMPROPER
ca-ca-ca-ct          1.1          180.0         2.0
ca-ca-ct-ca          1.1          180.0         2.0
ca-ca-ca-ss          1.1          180.0         2.0
c -ca-ca-ca          1.1          180.0         2.0
ca-o -c -o           1.1          180.0         2.0
c -c3-n -c3          1.1          180.0         2.0
ca-n -c -o          10.5          180.0         2.0
n -o -c -os          1.1          180.0         2.0

NONBOND
ct          1.9080  0.0860
```

MD-simulations in explicit water shell

The MD-simulations were carried out by means of the Amber20[7] software package using the parmbsc1[8] force field for DNA parts and the modified gaff force field for the rest (see above).

The initial unmodified DNA duplexes in the form of B-helices were obtained using the NAB utility from the AmberTools21 package. The modification and preparation of starting structures for the calculation was carried out using the "xaLeap" program. For each duplex with spin labels, four extended conformations were made corresponding to the *cis*-/*trans*- configurations of the piperazine linker and the *M*-/*P*- propellers of the trityl core. In each starting structure, the spin label was placed away from the duplex. Obtained anions were neutralized with sodium counterions, added to the shell using the Coulomb potential on the grid. Then the systems were solvated in rectangular TIP3P water boxes with the minimum solute–box boundary distance set to 12 Å. Periodic boundary conditions were imposed in the simulations using the Particle-Mesh Ewald method to treat the long-range electrostatic interactions with Coulomb cut-off distance 8 Å.

Obtained models were relaxed to create stable systems. This procedure included: 1) 10000 minimization steps with positional restraint 100 kcal/mol/Å^2 on DNA (except for two terminal residues on the trityl side, steepest descent algorithm); 2) 20000 steps unrestrained minimization; 3) slow heating up the system (Langevin dynamics with collision frequency 2 ps^{-1} and time step

of 0.5 fs), from 50 K to 300 K under constant volume with positional restraint 10 kcal/mol/Å^2 on solute for 0.5 ns; 4) relax the system (Langevin dynamics with collision frequency 2 ps^{-1} and time step of 1 fs) at a constant pressure 1.0 bar (the Monte Carlo barostat) at 300K with positional restraint 10 kcal/mol/Å^2 on solute for 0.5 ns; 5) relax the system (Langevin dynamics with collision frequency 2 ps^{-1} and time step of 1 fs) at a constant pressure 1.0 bar (the Monte Carlo barostat) at 300K for 0.5 ns.

Productive trajectories were obtained using the GPU (CUDA) version of PMEMD [9–11]. Two productive trajectories with different seeds (Langevin dynamics with collision frequency 2 ps^{-1} and time step of 2 fs) were obtained at a constant pressure 1.0 bar (Berendsen barostat, pressure relaxation time 2 ps) at 300K for 90-100ns and consisted of 10 ps snapshots. Analysis results are shown below.

Figure S6: "Unmodified" DNA-duplex DNA20-1

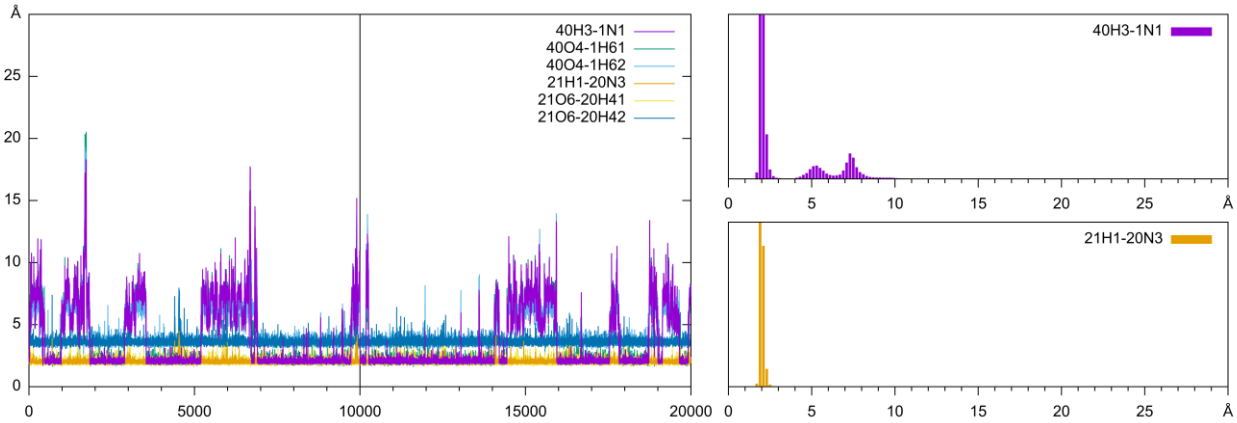

Figure S6. Results of MD simulation for the DNA duplex **DNA20-1**. On the left, concatenated visualization of the distances between pairs of atoms in the terminal pairs 40(DU3)-1(DA5) and 21(DG5)-20(DC3), obtained for two trajectories of 100 ns with a step of 0.1 ns. **On the right**, the pair-distance distribution between atoms forming the central hydrogen bond in Watson–Crick terminal base pairs 40(DU3)-1(DA5) (**top right**) and 21(DG5)-20(DC3) (**bottom right**). The proportion of the frayed structure (the distance between the 40H3 and 1N1 atoms > 4.0 Å) in the 40(DU3)–1(DA5) terminal pair was 34%.

Figure S7: Fluorine labeled DNA-duplex DNA20-F1

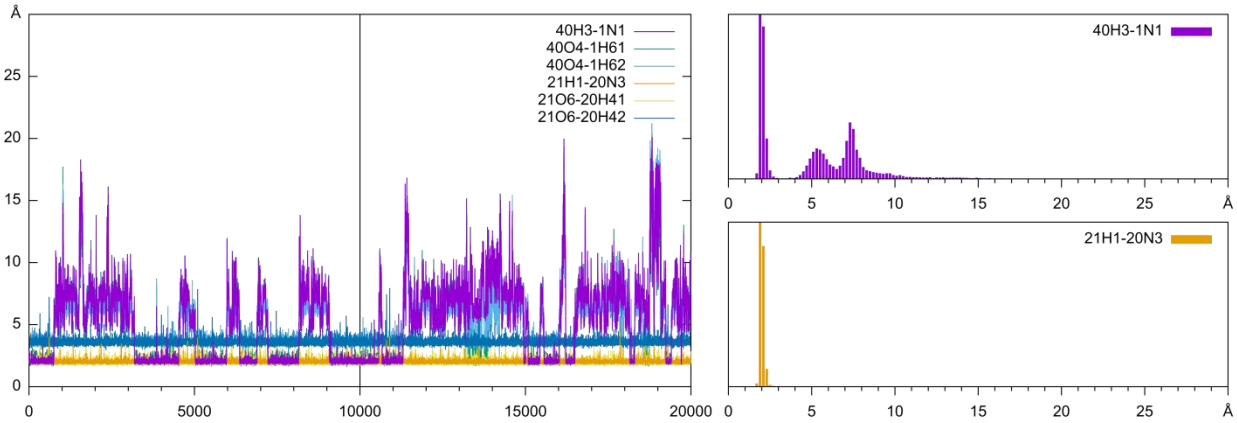

Figure S7. Results of MD simulation for the DNA duplex **DNA-20-F1**. The proportion of the frayed structure (the distance between the 40H3 and 1N1 atoms > 4.0 Å) in the 40(DU3)–1(DA5) terminal pair was 60%. Other details are the same as the Figure S6.

Figure S8. F- and Finland trityl labeled DNA-duplex Fin-DNA-20-F1 (τ=1600ns)

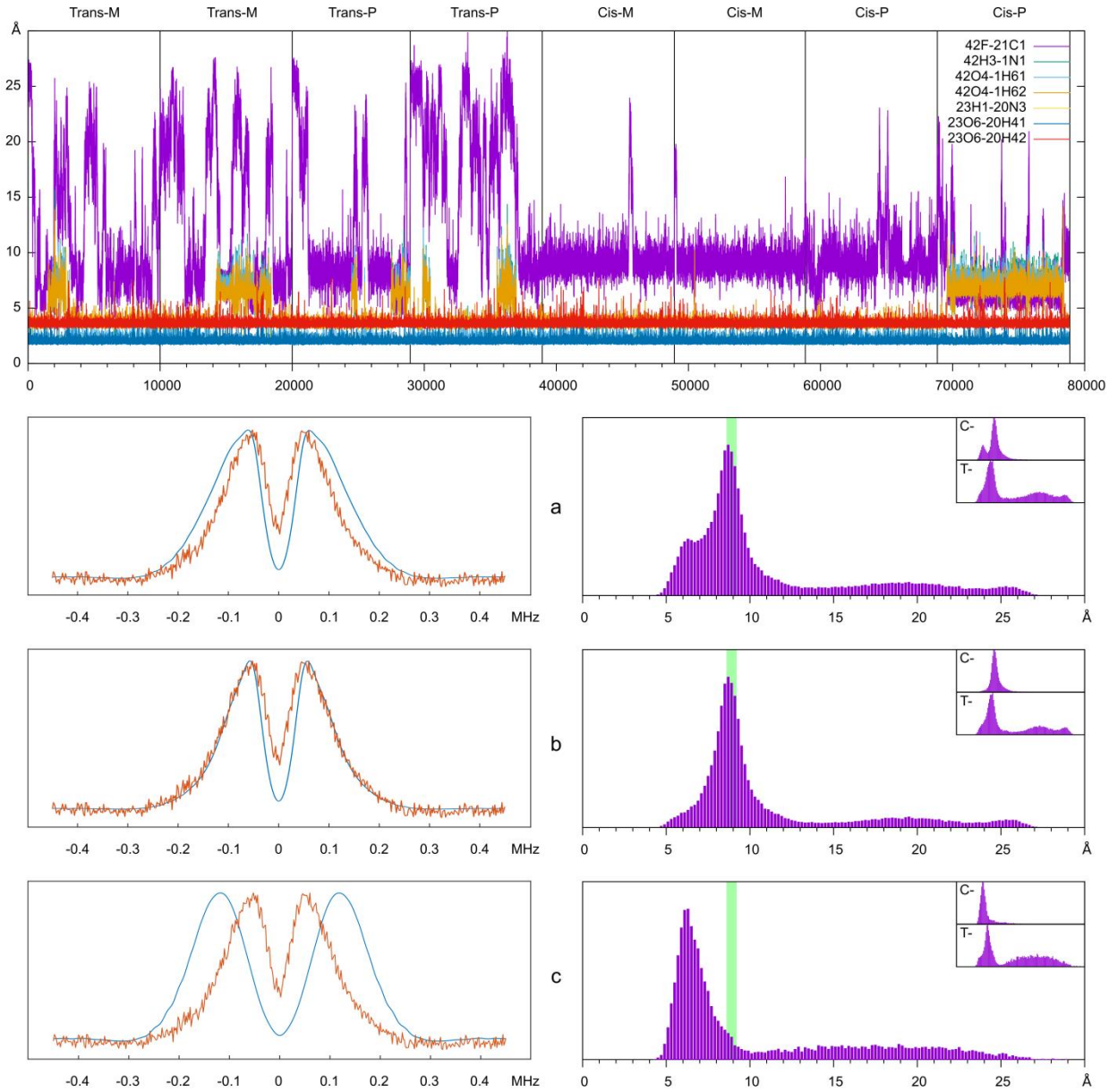

Figure S8. Results of MD simulation for the DNA duplex **Fin-DNA-20-F1** and comparison of the simulated Mims ENDOR spectra (τ=1600ns) with experiment. **On the top**, concatenated visualization of the distances of atoms in the terminal pairs 42(DU3)-1(DA5), 23(DG5)-20(DC3) and between F atom and a central carbon atom C1 of trityl fragment. For each structure (trans-/cis-configuration of amide bonds of the piperazine linker and P/M-trityl propeller), two trajectories with a duration of about 100 ns with a step of 0.1 ns were obtained. The proportion of the frayed structure (the distance between the 42H3 and 1N1 atoms > 4.0 Å) in the 42(DU3)–1(DA5) terminal pair was 24%. **a**,**b**,**c – left:** Comparison of the experimental (orange line) and simulated Mims ENDOR spectra (blue line). **a**,**b**,**c** – **right**: Corresponding pair distance distribution between F atom and a central carbon atom of trityl fragment. Inserts indicate distributions for cis- ("C-") and trans- ("T-") linker configuration separately. The green region marks the interval obtained from difference between the peaks of the experimental "doublet" (see R_{read} in the Table2 of main text). **a:** All structures are used. **b:** Only unfrayed structures are used **c:** Only frayed structures are used.

Figure S9. F- and Finland trityl labeled DNA-duplex Fin-DNA-20-F1 (τ=2500ns)

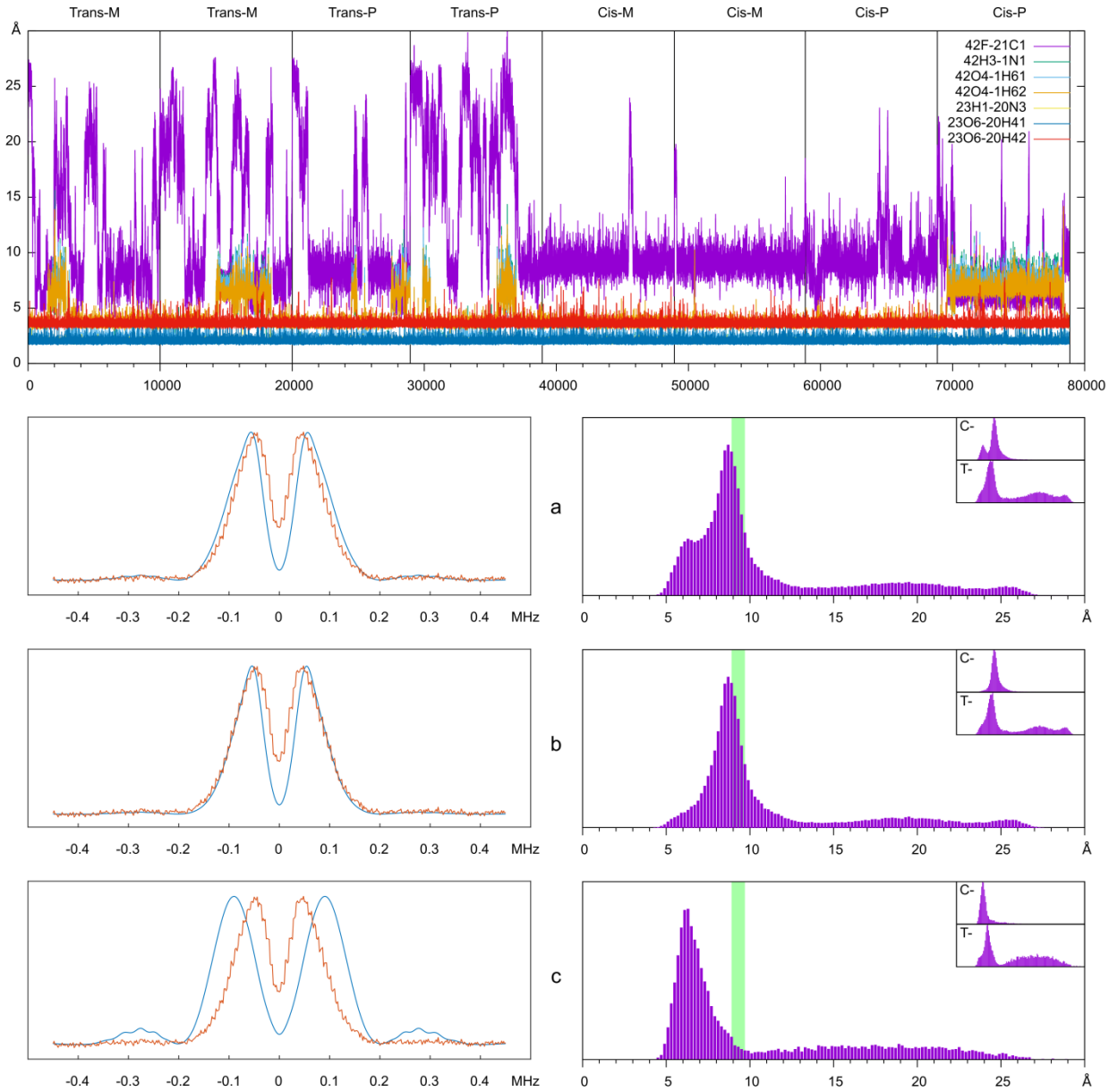

Figure S9. Results of MD simulation for the DNA duplex **Fin-DNA-20-F1** and comparison of the simulated Mims ENDOR spectra (τ=2500ns) with experiment. Other details are the same as the Figure S8.

Figure S10. F- and OX063 labeled DNA-duplex Oxo-DNA-20-F1 (τ=2500ns)

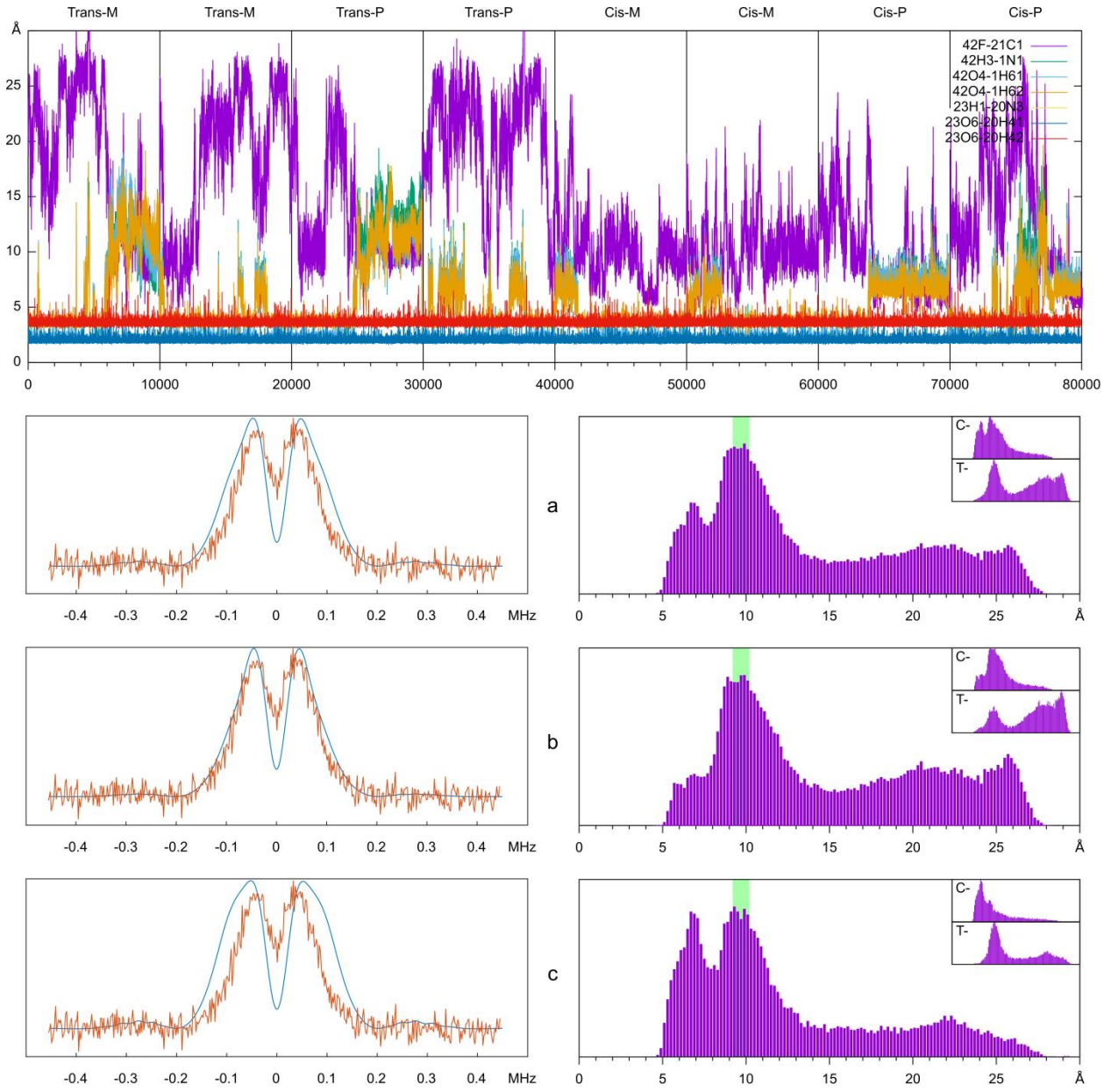

Figure S10. Results of MD simulation for the DNA duplex **OXO63-DNA-20-F1** and comparison of the simulated Mims ENDOR spectra (τ=2500ns) with experiment. The proportion of the frayed structure (the distance between the 42H3 and 1N1 atoms > 4.0 Å) in the 42(DU3)–1(DA5) terminal pair was 48%. Other details are the same as the Figure S8.

Figure S11. “Unmodified” DNA-duplex DNA20-2

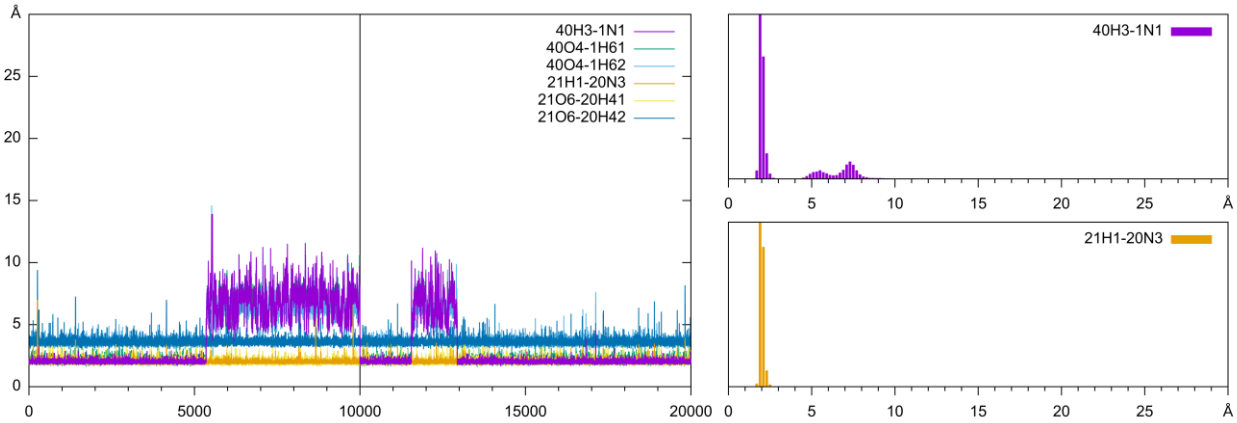

Figure S11. Results of MD simulation for the DNA duplex **DNA-20-2**. On the left, concatenated visualization of the distances between pairs of atoms in the terminal pairs 40(DT3)-1(DA5) and 21(DG5)-20(DC3), obtained for two trajectories of 100 ns with a step of 0.1 ns. On the right, the pair-distance distribution between atoms forming the central hydrogen bond in Watson–Crick terminal base pairs 40(DT3)-1(DA5) (top right) and 21(DG5)-20(DC3) (bottom right). The proportion of the frayed structure (the distance between the 40H3 and 1N1 atoms > 4.0 Å) in the 40(DT3)–1(DA5) terminal pair was 30%.

Figure S12. Fluorine labeled DNA-duplex DNA20-F2

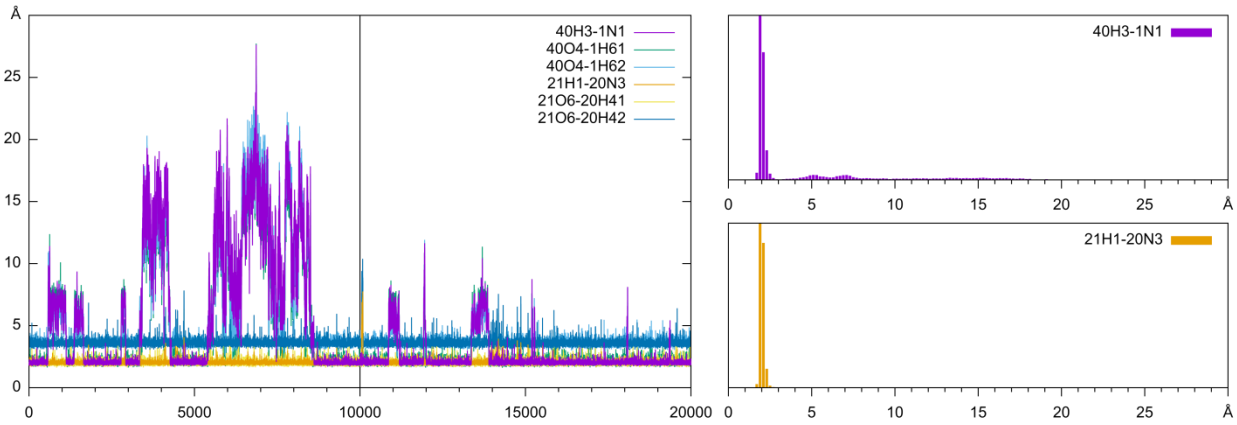

Figure S12. Results of MD simulation for the DNA duplex **DNA-20-F2**. The proportion of the frayed structure (the distance between the 40H3 and 1N1 atoms > 4.0 Å) in the 40(DT3)–1(DA5) terminal pair was 30%. Other details are the same as the Figure S11.

Figure S13. F- and Finland trityl labeled DNA-duplex Fin-DNA-20-F2 (τ=2000ns)

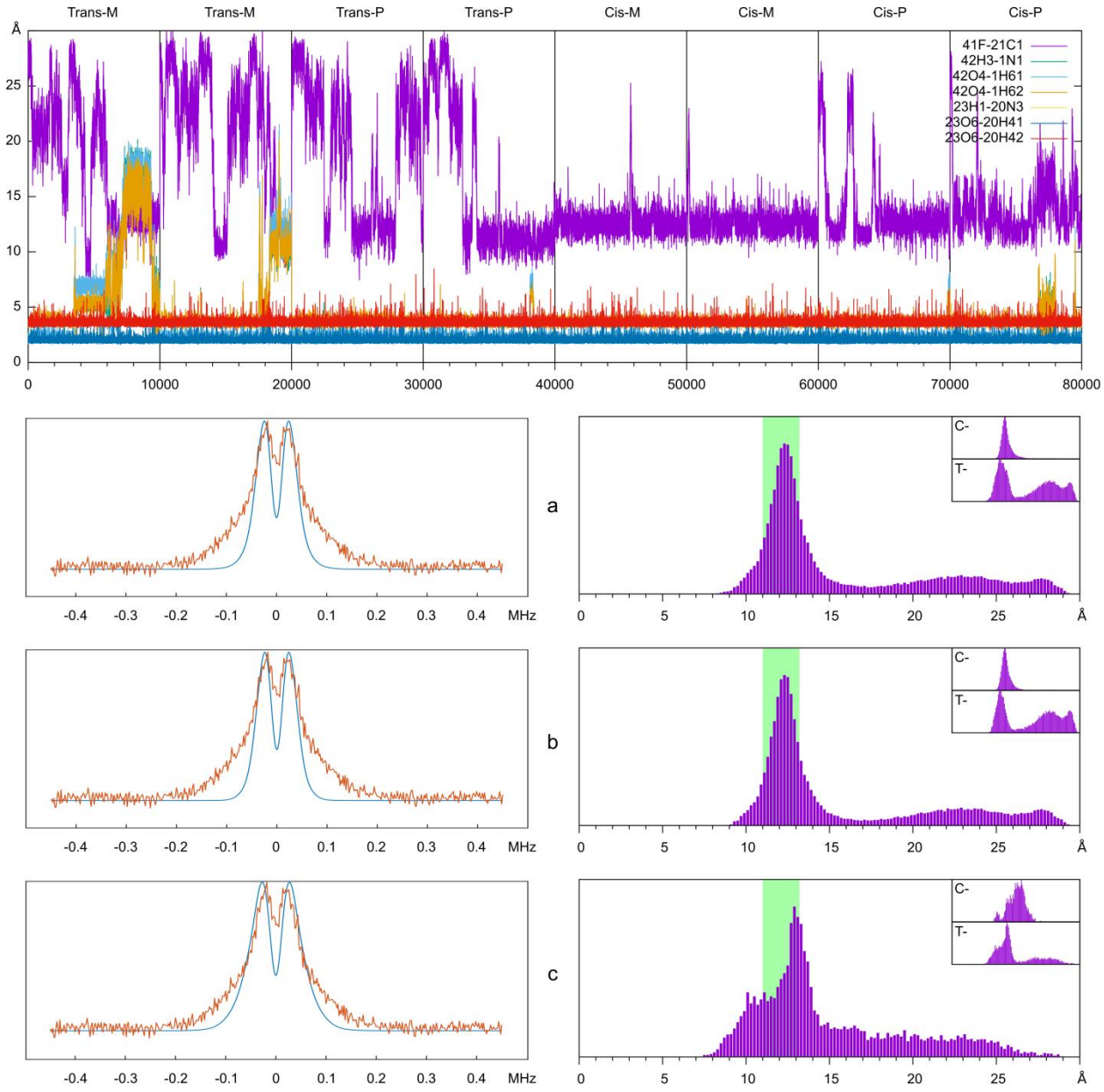

Figure S13. Results of MD simulation for the DNA duplex **Fin-DNA-20-F2** and comparison of the simulated Mims ENDOR spectra (τ=2000ns) with experiment. On the top, concatenated visualization of the distances of atoms in the terminal pairs 42(DT3)-1(DA5), 23(DG5)-20(DC3) and between F atom and a central carbon atom C1 of trityl fragment. For each structure (trans-/cis-configuration of amide bonds of the piperazine linker and P/M-trityl propeller), two trajectories with a duration of about 100 ns with a step of 0.1 ns were obtained. The proportion of the frayed structure (the distance between the 42H3 and 1N1 atoms > 4.0 Å) in the 42(DT3)–1(DA5) terminal pair was 10%. **a,b,c – left:** Comparison of the experimental (orange line) and simulated Mims ENDOR spectra (blue line). **a,b,c – right:** Corresponding pair distance distribution between F atom and a central carbon atom of trityl fragment. Inserts indicate distributions for cis- ("C-") and trans- ("T-") linker configuration separately. The green region marks the interval obtained from difference between the peaks of the experimental "doublet" (see R_{read} in the Table2 of main text). **a:** All structures are used. **b:** Only unfrayed structures are used. **c:** Only frayed structures are used.

Figure S14. F- and OXO63 labeled DNA-duplex OX0-DNA-20-F2 (τ=2500ns)

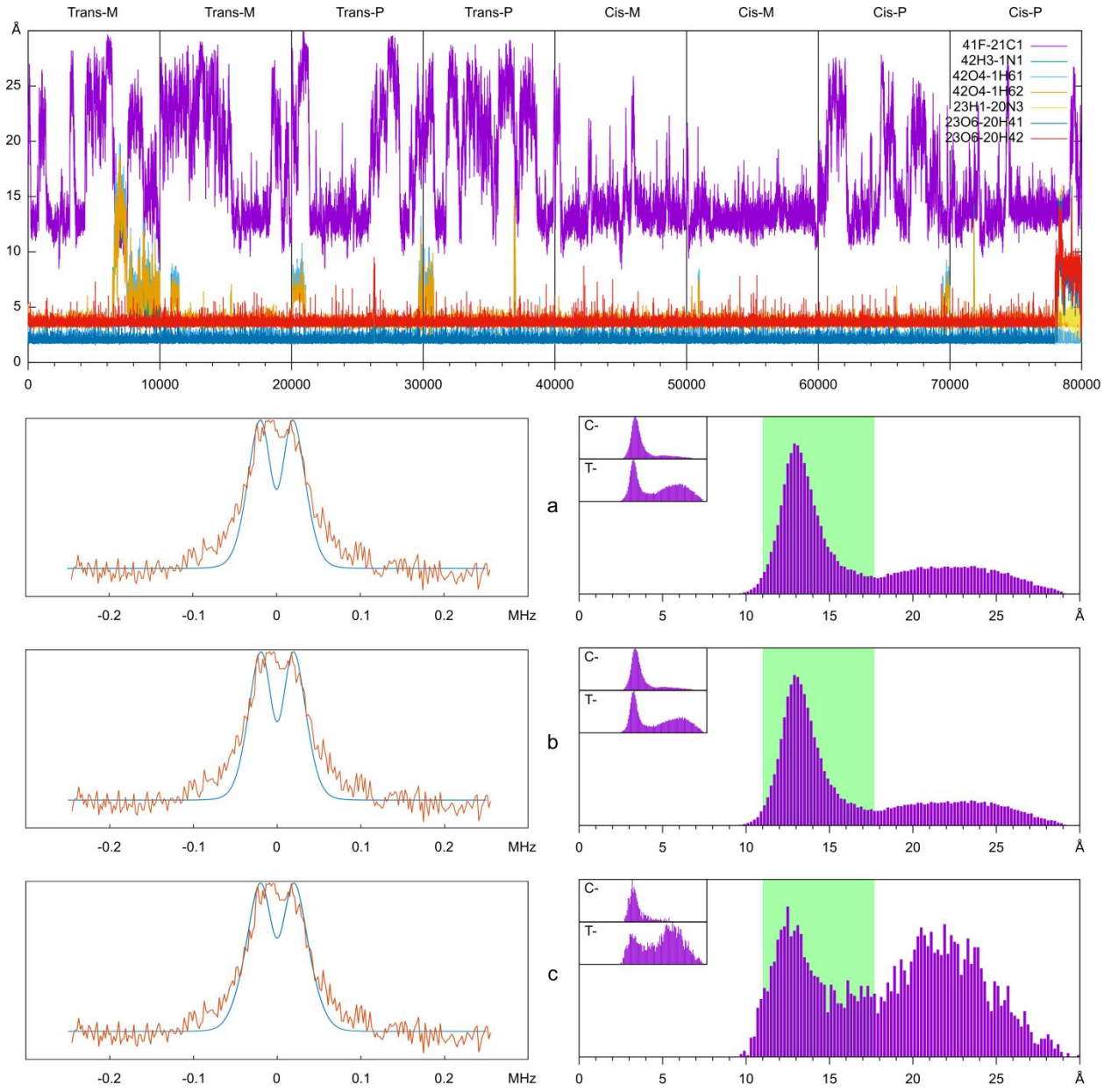

Figure S14. Results of MD simulation for the DNA duplex **OXO63-DNA-20-F2** and comparison of the simulated Mims ENDOR spectra (τ=2500ns) with experiment. The proportion of the frayed structure (the distance between the 42H3 and 1N1 atoms > 4.0 Å) in the 42(DT3)–1(DA5) terminal pair was 7%. Other details are the same as the Figure S13.

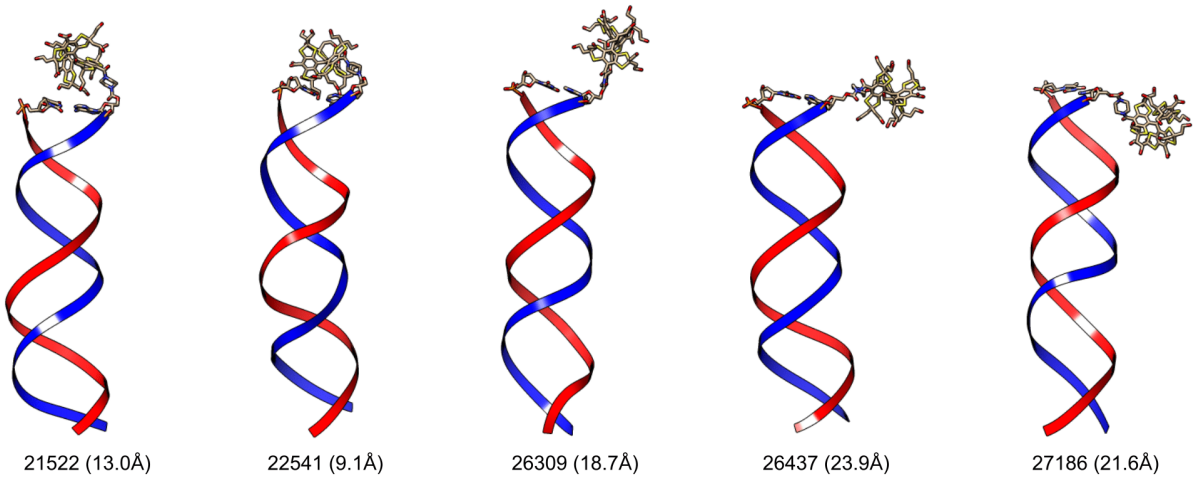

Figure S15. Representative snapshots from the Figure S14. The distance between the F atom and the central C1 carbon atom of the trityl fragment is shown in parentheses. Hydrogen atoms omitted from sticks for clarity.

References

1 A. Meyer, S. Dechert, S. Dey, C. Höbartner and M. Bennati, Measurement of Angstrom to Nanometer Molecular Distances with 19F Nuclear Spins by EPR/ENDOR Spectroscopy, *Angew. Chemie - Int. Ed.*, 2020, **59**, 373–379.

2 C. Gemperle and A. Schweiger, Pulsed electron-nuclear double resonance methodology, *Chem. Rev.*, 1991, **91**, 1481–1505.

3 S. Grimme, A. Hansen, S. Ehlert and J.-M. Mewes, r2SCAN-3c: A “Swiss army knife” composite electronic-structure method, *J. Chem. Phys.*, 2021, **154**, 64103.

4 F. Neese, F. Wennmohs, U. Becker and C. Riplinger, The ORCA quantum chemistry program package, *J. Chem. Phys.*, 2020, **152**, 224108.

5 M. Bursch, J.-M. Mewes, A. Hansen and S. Grimme, Best-Practice DFT Protocols for Basic Molecular Computational Chemistry, *Angew. Chemie Int. Ed.*, 2022, **61**, e202205735.

6 G. M. J. Barca, C. Bertoni, L. Carrington, D. Datta, N. De Silva, J. E. Deustua, D. G. Fedorov, J. R. Gour, A. O. Gunina, E. Guidez, T. Harville, S. Irle, J. Ivanic, K. Kowalski, S. S. Leang, H. Li, W. Li, J. J. Lutz, I. Magoulas, J. Mato, V. Mironov, H. Nakata, B. Q. Pham, P. Piecuch, D. Poole, S. R. Pruitt, A. P. Rendell, L. B. Roskop, K. Ruedenberg, T. Sattasathuchana, M. W. Schmidt, J. Shen, L. Slipchenko, M. Sosonkina, V. Sundriyal, A. Tiwari, J. L. Galvez Vallejo, B. Westheimer, M. Włoch, P. Xu, F. Zahariev and M. S. Gordon, Recent developments in the general atomic and molecular electronic structure system, *J. Chem. Phys.*, 2020, **152**, 154102.

7 D. A. Case, K. Belfon, I. Y. Ben-Shalom, S. R. Brozell, D. S. Cerutti, T. E. Cheatham, V. W. D. C. III, T. A. Darden, R. E. Duke, G. Giambasu and others, AMBER2020, university of California, San Fransisco, *J. Amer. Chem. Soc*, 2020, **142**, 3823–3835.

8 I. Ivani, P. D. Dans, A. Noy, A. Pérez, I. Faustino, A. Hospital, J. Walther, P. Andrio, R. Goñi, A. Balaceanu, G. Portella, F. Battistini, J. L. Gelpí, C. González, M. Vendruscolo, C. A. Laughton, S. A. Harris, D. A. Case and M. Orozco, Parmbsc1: a refined force field for DNA simulations, *Nat. Methods*, 2016, **13**, 55–58.

9 A. W. Gotz, M. J. Williamson, D. Xu, D. Poole, S. Le Grand and R. C. Walker, Routine microsecond molecular dynamics simulations with AMBER on GPUs. 1. Generalized born, *J. Chem. Theory Comput.*, 2012, **8**, 1542–1555.

10 R. Salomon-Ferrer, A. W. Gotz, D. Poole, S. Le Grand and R. C. Walker, Routine microsecond molecular dynamics simulations with AMBER on GPUs. 2. Explicit solvent particle mesh Ewald, *J. Chem. Theory Comput.*, 2013, **9**, 3878–3888.

11 S. Le Grand, A. W. Götz and R. C. Walker, SPFP: Speed without compromise—A mixed precision model for GPU accelerated molecular dynamics simulations, *Comput. Phys. Commun.*, 2013, **184**, 374–380.